Pergamon

Electrochimica Acta, Vol. 43, Nos 19–20, pp. 2899–2909, 1998

Printed in Great Britain
PII: S0013-4686(98)00030-9
0013-4686/98 $19.00 + 0.00

Anion and electrode surface structure effects on the deposition of metal monolayers: electrochemical and time-resolved surface diffraction studies

H. D. Abruña,[a]* J. M. Feliu,[c] J. D. Brock,[b] L. J. Buller,[a] E. Herrero,[a,c] J. Li,[a] R. Gómez[c] and A. Finnefrock[b]

[a]Department of Chemistry, Cornell University, Ithaca, NY 14853, U.S.A.

[b]Applied and Engineering Physics, Cornell University, Ithaca, NY 14853, U.S.A.

[c]Departamento de Química-Física, Universitat d'Alacant, E-03080 Alacant, Spain

(Received in Newcastle 21 January 1998)

Abstract—The effects of anions and electrode surface structure on the UPD of metal monolayers are illustrated with three different examples. In the first, we show that for Cu UPD on Pt[n(111) × (110)] (n = 2, 3, 5, 9 and 19) stepped surfaces in sulfuric acid medium, submonolayer amounts of underpotentially deposited copper induce the adsorption of (bi)sulfate in the vicinity of copper adatoms deposited on (110) step sites. The induced anion adsorption increases with terrace width up to a three Pt atoms wide terrace, suggesting that this is the minimum width to accommodate the copper adatom and the coadsorbed anion. In the second case we present data from simultaneous time-resolved surface X-ray scattering and chronoamperometric measurements of Cu UPD on Pt(111) electrodes in the presence of chloride anions. These studies demonstrate that the kinetics of formation of the incommensurate CuCl adlayer from the commensurate (1 × 1) Cu layer takes place in a much longer time scale than the current response. This is a clear indication of the temporal separation (resolution) between electrochemical events and processes associated with surface reorganization to achieve long-range periodic ordering. Finally, we consider the UPD of Hg on Au(111) electrodes with emphasis on the relationship between the partial charge retained by the mercury and anion adsorption. At the early stages of Hg UPD, when mercury is still partially charged, an ordered mercurous–sulfate bilayer structure is formed on the electrode surface. At more negative potentials, where mercury is almost fully discharged, two additional ordered hexagonal mercury adlayers are formed with little, if any, interactions with the anions, suggesting that the interactions between them are largely electrostatic in nature.

Key words: underpotential deposition, Au and Pt single crystals, anion and electrode structure effects, surface X-ray scattering.

INTRODUCTION

The UPD (underpotential deposition) of metals onto foreign metal substrates has been widely studied in recent years, in part because such studies provide a way to investigate the early stages of metal deposition and the different factors that affect it. The main driving force for the UPD processes is the interaction between the metal to be deposited and the foreign metal substrate [1, 2]. For that reason, UPD phenomena are generally restricted to the deposition of one monolayer prior to bulk deposition, although in some cases, up to three layers can be deposited.

Although the main driving force for the UPD processes is the metal–substrate interaction, other interactions can also play an important role in the process. The presence of strongly adsorbing anions in the electrolyte has particular importance, since the anion–metal and anion–substrate interactions

*Author to whom correspondence should be addressed.

can significantly modify UPD processes [1, 2]. Depending on the strength of the anion interactions and their relative magnitude when compared with the metal–substrate interactions, different effects can be observed. In some cases, strongly adsorbing anions delay the UPD process since the first atoms to be deposited have to displace the anions form the surface [3]. On the other hand, the opposite is also possible; some UPD processes appear at more positive potentials in the presence of strongly adsorbing anions due to the stability effect that a strong interaction between the adsorbed metal and the anion has on the adlayer [4]. In other cases, the effect of the anion is to alter the kinetics of the UPD process with virtually no change in the potential for the UPD process [5, 6].

An additional complication in UPD processes is that the deposited metal is almost never fully discharged in the early stages of deposition [7–10]. In fact, the deposited metal goes from being partially discharged at the early stages to being fully discharged when the applied potential is close to that for bulk deposition. The changing charge state of the metal causes a change in its interactions with the anion. At more positive potentials, where the metal still retains a partial charge, there is a strong attractive electrostatic interaction between the anion and the deposited metal that disappears when the metal in fully discharged. This type of attractive interaction often gives rise to the appearance of a metal–anion bilayer deposited on the electrode surface at intermediate potentials [4, 11–13].

It is clear that strongly adsorbing anions can alter UPD process, but the opposite can also take place; the UPD process may also modify the interactions between the substrate and the anion. For example, this is the case for Cu UPD on Pt(111) electrodes in the presence of chloride and bromide anions [14]. The initial stages of Cu UPD on the electrode surface bring about an induced adsorption of the anion at sites neighboring an electrodeposited Cu atom.

Additionally, the structural details of the surface also affect UPD processes. This is particularly evident when deliberately stepped surfaces are employed. In a recent study of Cu UPD on Pt(311) (Pt(311) = Pt[2(111) × (100)] we found that the deposition/stripping processes occurred in two stages related to the presence of (100) steps and (111) terraces [15]. It appeared that copper was more stable when adsorbed on the terraces relative to the steps. The unambiguous identification of the specific sites of adsorption/deposition was only possible by using low concentrations of copper as well as relatively high sweep rates in order to monitor this selective adsorption as a function of coverage at or below monolayer levels. Clearly, there is a delicate interplay among all of these interactions, which affect UPD processes.

In this paper, we present three examples of anion and electrode surface structure effects on UPD processes. The specific systems to be discussed are: (i) induced adsorption of (bi)sulfate anions by Cu UPD on Pt[n(111) × (110)] (n = 2, 3, 5, 9 and 19) stepped surfaces (general notation Pt(n + 1, n + 1, n − 1)), (ii) distinction of time scales involved in electrochemical processes of Cu UPD on Pt(111) in the presence of chloride vs surface ordering to form an ordered CuCl bilayer and (iii) changes in the anion–adlayer interaction in Hg UPD on Au(111) electrodes as the partial charge of the deposited mercury is varied.

EXPERIMENTAL

Pt(111) and Au(111) single crystals (~9 mm in diameter and ~2 mm thick) used as working electrodes for the X-ray scattering measurements were grown from the melt at the materials preparation facility at Cornell University. They were first oriented through X-ray diffraction and mechanically polished so that the crystal surfaces were within 0.3° of the (111) plane. The platinum stepped surfaces were prepared according to Clavilier's technique with a miscut of less than 0.1° [16]. Prior to any measurement, the electrodes were flame-annealed, quenched with ultrapure water and transferred to the cell for electrochemical measurements. For the platinum stepped surfaces, the electrode was cooled after the flame treatment in a N_2/H_2 (95/5) atmosphere, since it minimizes the presence of surface defects [17, 18].

X-ray diffraction experiments were performed at the X10Å and B and X20Å beamlines at the National Synchrotron Light Source using a four circle diffractometer. Energy of 8.80 and 10.90 keV were employed for Cu UPD on Pt(111) electrodes and Hg UPD on Au(111) electrodes, respectively. The sample cell has a reflection geometry and is similar to those used by others in previous studies [19–21]. X-ray photons penetrate through a 2.5 μm Mylar film (Chemplex) as well as a thin film of electrolyte (estimated to be about 30 μm) covering the Pt(111) and Au(111) crystals. To prevent the diffusion of oxygen from air through the Mylar film, an outer shield with a Kapton window (Chemplex) was placed on top of the sample cell and continuously flushed with ultra pure N_2. Cyclic voltammograms in the X-ray cell were carried out with the Mylar film inflated by adding deoxygenated electrolyte solution. For X-ray measurements, some electrolyte solution was withdrawn so that the Mylar film was pressed against the crystal surface thus achieving a thin layer configuration. Pt(111) and Au(111) surfaces are described in terms of a hexagonal lattice with the c axis along the ⟨111⟩ direction with $a = b = 2.774$ Å for platinum and $a = b = 2.885$ Å for gold, respectively.

All experiments were carried out at room temperature. Solutions were prepared using ultrapure water (18 MΩ Millipore® Milli-Q® water), $HClO_4$ (doubly distilled, GFS), H_2SO_4 (Merck Suprapur or Ultrex, Baker), NaCl (99.999%, Aldrich), CuO (Aldrich, 99.999%) CH_3COOH (99.9985%, Alfa), CH_3COONa (99.999%, Alfa), and HgO (99.998%, Alfa).

RESULTS AND DISCUSSION

Cu UPD on Pt[*n*(111) × (110)] stepped surfaces in the presence of bisulfate anions

In these studies, we employed an approach similar to that described earlier for Cu UPD on Pt(311) [15]. The surfaces studied include the Pt(111) and (110) surfaces and the stepped surfaces of (10,10,9), (554), (332), (221) and (331), which correspond to terrace widths of 19, 9, 5, 3 and 2 atoms respectively, with monatomic (110) steps. In a typical experiment, the electrode was immersed in a solution containing 0.1 M $H_2SO_4 + 1.0 \times 10^{-5}$ M Cu^{2+} at a potential were Cu UPD does not take place. The electrode potential was then cycled over a range where Cu is deposited at a transport-limited rate but where its stripping did not occur. Due to the low Cu concentration (10 μM), Cu accumulates slowly on the electrode surface so that the changes in the voltammetric profile can be easily monitored. At specific intervals, the Cu is stripped from the electrode surface to determine its surface coverage.

Figure 1 shows the voltammetric profile of a Pt(111) electrode in contact with the above mentioned solution. As can be readily seen, increasing amounts of Cu (deposited in each cycle) lead to a diminution of both the usual and unusual adsorption states of the Pt(111) surface, until the electrode surface is completely blocked (not shown in the figure). The only (small) difference with respect to the voltammetric profile of a Pt(111) electrode in 0.1 M H_2SO_4 is the appearance of a small bump at *ca.* +0.25 V vs NHE. This has been previously observed and attributed to anion induced adsorption [3, 22]. However, when the experiment was repeated in 0.1 M $HClO_4 + 1.0 \times 10^{-5}$ M Cu^{2+}, the voltammetric profile in the region around +0.25 V was identical to that of Fig. 1. This observation indicates that (bi)sulfate anions are not responsible for the appearance of this feature at +0.25 V. Compared with the results obtained in the presence of chloride or bromide anions on Pt(111) [14], it is evident that the presence of induced adsorption depends on the nature of the anion. Very similar behavior was exhibited by a Pt(110) electrode [23], were no induced adsorption was observed.

The stepped surfaces present a quite different situation. Figure 2 shows the voltammetric behavior of different platinum stepped surfaces ((a) Pt(554),

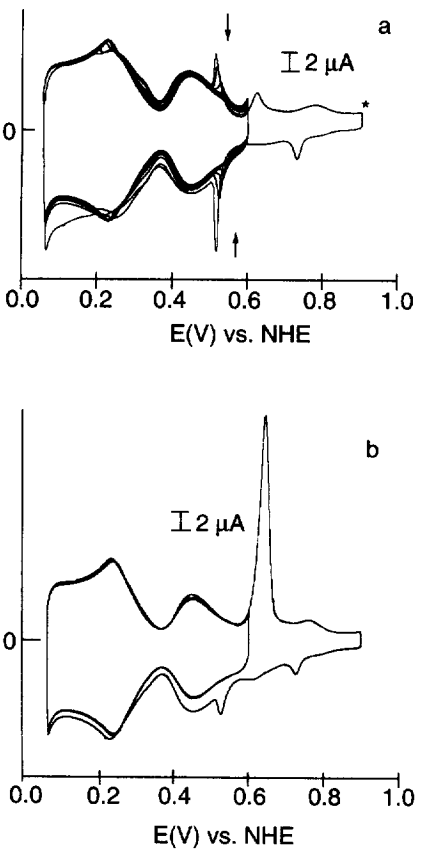

Fig. 1. (a) Successive voltammetric profiles (first cycle is denoted by (*) for a Pt(111) electrode in 0.1 M $H_2SO_4 + 1.0 \times 10^{-5}$ M Cu^{2+} after the positive limit is lowered to +0.60 V. (b) Stripping of the copper previously electrodeposited. v = 50 mV s^{-1}

(b) Pt(332), (c) Pt(221) and (d) Pt(331)) in contact with a 0.1 M $H_2SO_4 + 1.0 \times 10^{-5}$ M Cu^{2+} solution. The voltammetric profiles of these stepped surfaces in the absence of copper have been previously described extensively [24, 25]. In the first stages of copper deposition, a diminution of the signal at +0.18 V (which corresponds to hydrogen adsorption/desorption on the Pt(110) step sites [24]) is observed concomitant with the appearance (and subsequent increase) of a new wave at +0.25 V. This peak reaches it maximum when the step sites have been completely blocked by the deposited copper. Up to this instant, the signal corresponding to hydrogen adsorption on the (111) terrace sites remained constant, a clear indication that Cu electrodeposition is taking place preferentially at step sites. Moreover, good agreement was obtained between the Cu coverage measured from its stripping charge (once the peak at +0.25 reached its maximum amplitude) and the calculated coverage for a species covering only the step sites (Table 1). The only significant deviation from this behavior

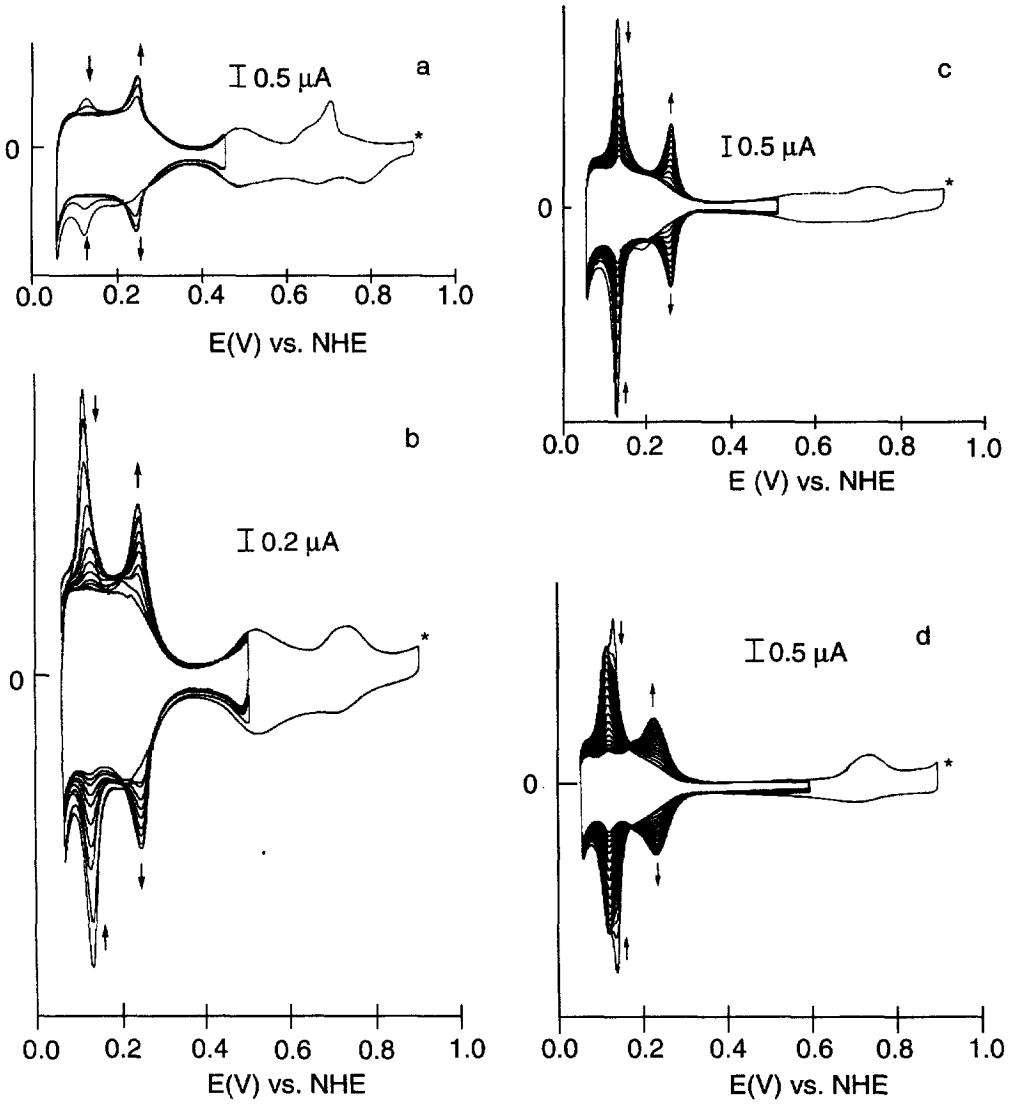

Fig. 2. Successive voltammetric profiles (first cycle is denoted by (*) for (a) Pt(554), (b) Pt(332), (c) Pt(221) and (d) Pt(331) electrodes in 0.1 M $H_2SO_4 + 1.0 \times 10^{-5}$ M Cu^{2+} after the positive limit is lowered below 0.60 V. $v = 50$ mV s^{-1}

Table 1.
Coulometric charges and fractional coverages during Cu UPD on stepped surfaces in sulfuric acid medium

Surface	Charge of the induced adsorption peak at maximum amplitude (μC cm^{-2})	Cu stripping charge at maximum induced adsorption (μC cm^{-2})	Cu coverage at maximum induced adsorption*	Ratio of step sites to total number of sites
(111)	–	0	0	0
(10, 10, 9)	–	0	0	1:19 (0.05)
(554)	14	63	0.13	1:9 (0.11)
(332)	31	106	0.23	1:5 (0.20)
(221)	41	126	0.29	1:3 (0.33)
(331)	36	101	0.26	1:2 (0.50)
(110)	–	0	0	–

*We are aware that the Cu stripping charge contains contributions associated to anion adsorption/desorption. Two terms can be considered, the (bi)sulfate desorption from the adsorbed (bi)sulfate induced by the copper on the step and the (bi)sulfate adsorption onto the platinum surface once copper has been stripped. Since both correction terms have opposite sign and it is not clear which one it is dominant, we give uncorrected charge values.

was observed for the surface with the lowest terrace width (2 atoms) Pt(331) (*vide infra*).

Once all the step sites have been covered by Cu, additional Cu atoms are deposited on terrace sites. With further cycling, the signal from hydrogen adsorption/desorption on terrace sites starts diminishing along with the peak at +0.25 V. This, again, implies that the peak at +0.25 V is associated with the presence of copper on the step sites and that it reaches a maximum when they are all covered with copper.

In principle, the development of the new voltammetric feature at +0.25 V could be attributed to the adsorption/desorption of any of the several species present in solution: HSO_4^-/SO_4^{2-}, H_3O^+, or Cu^{2+}. From previous work we can discard H_3O^+ as a possible candidate [14], since in perchloric acid this feature is absent. It is also unlikely that copper is directly responsible for these adsorption states due to the sharpness and reversibility of the new peaks; especially in light of the low Cu concentration. Therefore we conclude that the peaks are associated with the induced adsorption/desorption of (bi)sulfate by copper deposited on the step sites. While the potential of this new peak was not dependent on copper coverage, its amplitude was. The maximum amount of induced adsorption was strongly dependent on terrace width with the (221) surface exhibiting the largest extent of induced adsorption. This surface appears to have the minimum amount of space on the terrace needed to accommodate both deposited copper adatoms and induced adsorbed anions. For surfaces with terrace widths larger than 3 atoms, the amount of induced adsorption scales with the step-site density as shown in Table 1. For the Pt(331) surface, with a two atoms wide terrace, there is a dramatic difference in the measured vs calculated values (Table 1) indicating that there is not sufficient space to accommodate both the deposited copper and the adsorbed (bi)sulfate. These studies illustrate the sensitivity of UPD processes to both the nature of the anion and the structure of the substrate.

Time-resolved surface X-ray scattering during copper UPD on Pt(111) in the presence of chloride anions

As mentioned earlier and as reported in numerous cases previously, the nature of the anions present in solution can have dramatic effects on UPD processes. In the second example we present results from a study of the kinetics of the formation of an ordered adlayer of UPD copper on a Pt(111) electrode in the presence of chloride anions. In particular, we have been able to carry out time-resolved surface X-ray scattering while simultaneously recording the current–time transient following a potential step. The UPD of copper on Pt(111) in the presence of chloride anions is well known and consists of two sharp and well defined voltammetric peaks centered at about +0.50 and +0.35 V (vs Ag/AgCl) and which correspond to the initial formation of an incommensurate CuCl bilayer after the first peak [13] and a commensurate copper monolayer after the second. The copper monolayer is, in turn, covered by a disordered layer of chloride anions [26–28].

In this particular study, we were interested in measuring the kinetics of formation and dissolution of the incommensurate CuCl bilayer structure by carrying out time-resolved surface X-ray scattering simultaneously with chronoamperometric current–time transients.

Figure 3 shows the cyclic voltammetric profile of Cu UPD on a Pt(111) electrode in the X-ray cell, in 0.1 M $HClO_4$ containing 1 mM Cu^{2+} and 10 mM Cl^-. Although the configuration is not ideal for electrochemical work due to ohmic drops and contributions from the edges of the crystal (making the peaks rather broad), the voltammetric profile is essentially the same as that previously reported [3, 26, 29] and consisted of two well-defined peaks centered at +0.54 and +0.30 V (vs Ag/AgCl) and reflecting the processes previously mentioned. These processes are completely reversible and stable for hours so that data acquisition can be carried out until the adequate statistics are obtained.

The real-time dynamics of the structural transition between the two ordered layers can be followed by monitoring the diffraction intensity at the (0.765, 0, 1.5) rod due to the presence of the CuCl bilayer. Figure 4 presents scans at +0.35 and +0.20 V which correspond to potential values where the CuCl bilayer is present or absent, respectively. At +0.35 V, a sharply defined peak is observed whereas at +0.20 V the peak is absent. These changes were reversible and could be

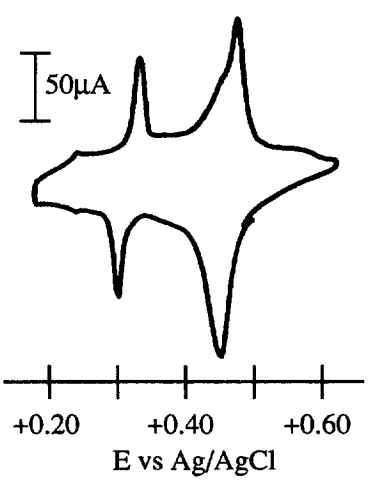

Fig. 3. Voltammetric profile for a Pt(111) electrode in contact with 0.1 M $HClO_4$ + 10 mM Cl^- + 1.0 mM Cu^{2+} in the *in situ* X-ray cell in the thin layer configuration. $v = 10\ mV\ s^{-1}$

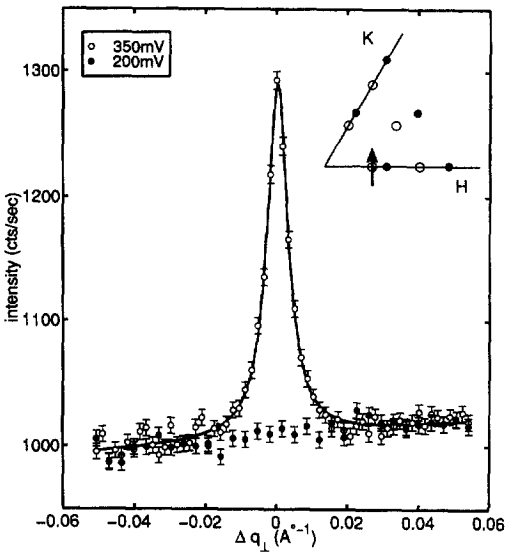

Fig. 4. Comparison of the scattered X-ray at the (0.765, 0, 0.5) (which corresponds to the incommensurate CuCl overlayer on Pt(111) electrodes and is shown in the inset by a cross) at +0.35 and +0.20 V

observed for periods of hours. The inset in Fig. 4 is derived from static X-ray scattering studies by Tidswell *et al.* [13]. Solid dots represent rods of scattering from the truncated Pt(111) surface, while hollow dots represent scattering from the incommensurate CuCl bilayer.

To study the dynamics of these structural transitions, the potential sequence in Fig. 5(a) was employed. At the initial potential, +0.20 V, the commensurate copper adlayer is present on the electrode surface. At t = 5 s, the potential is stepped to +0.35 V giving rise to the formation of the incommensurate CuCl layer. The potential is then stepped back to the initial value of +0.20 V at t = 25 s. This cycle is repeated in order to obtain appropriate statistics for the simultaneous surface X-ray scattering measurements.

Figure 5(b) shows the transient currents obtained for the potential step sequence in Fig. 5(a). As can be seen, the time for the decay of the current transient (due to the process of Cu dissolution/deposition and the reorganization of the chloride adlayer on the electrode surface) was well below 1 s following the step. The time evolution of the scattered X-ray intensity (Fig. 5(c)), however, was markedly different. In the case of the formation of the incommensurate CuCl adlayer, the development of the long-range periodic order requires a significantly longer time than that required for the electrodeposition. This implies that the processes of copper and anion adsorption/desorption and the formation of the ordered CuCl adlayer occur on very different time scales. On the other hand, the dissolution of the incommensurate structure (at +0.20 V) follows the current response. This is clearly observed in Fig. 5(c) where the leading part of the transient is significantly slower than the trailing part. Thus, it appears that in the formation of the incommensurate CuCl adlayer from the epitaxial Cu adlayers one can clearly separate the electrochemical response associated with copper desorption and the reorganization of the adsorbed chloride from the formation of the ordered CuCl bilayer structure which occurs over a much longer time scale.

Hg UPD on Au(111) electrodes in the presence of bisulfate anions

In the last example we employ the mercury UPD process on Au(111) electrodes to illustrate the effects of the partial charge retained by the metal on the interactions between the adsorbed metal and the anion. Figure 6 shows the voltammetric profile of an Au(111) electrode in contact with a 0.10 M H_2SO_4 + 0.1 mM Hg^{2+} solution. There are three prominent features in the CV. The main panel shows the cyclic voltammogram when the potential is cycled between +0.60 and +1.00 V, where two sets of very sharp peaks at +0.90 and +0.88 V can be observed. These features are stable and reproducible over the potential range between +0.60 and +1.00 V. The cathodic peaks are somewhat broadened due to the relatively low Hg^{2+} solution concentration.

Upon further scanning the potential to more negative values, a broad and diffusional-like re-

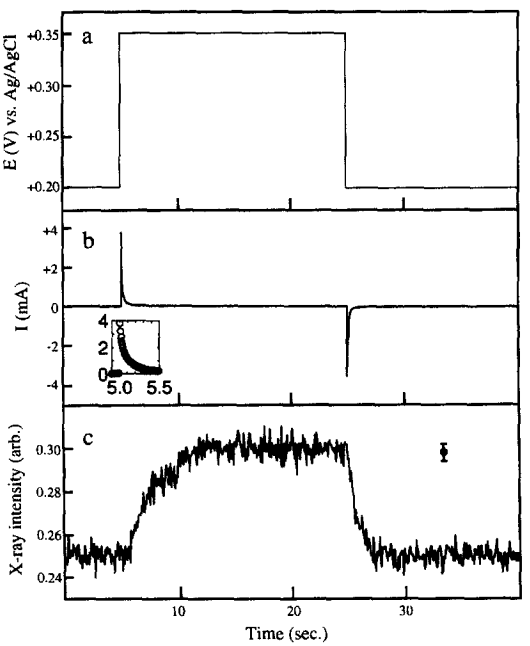

Fig. 5. (a) Applied potential sequence for the *in situ* X-ray experiments. (b) Current/time response (inset: transient at t = 5 s on an expanded scale). (c) Time dependence of the scattered X-ray intensity at (0.765, 0, 1.5)

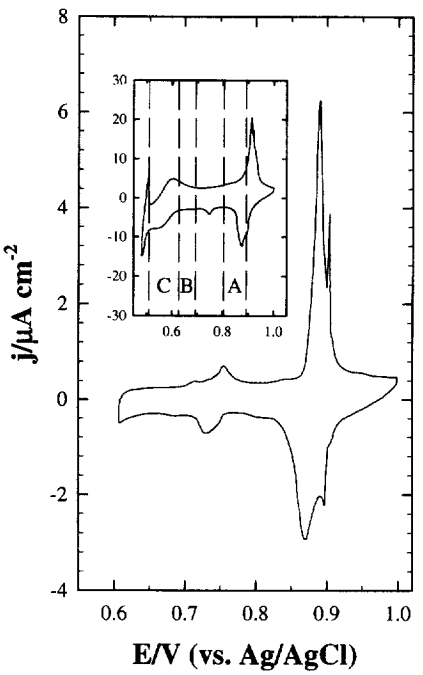

Fig. 6. Voltammetric profile of an Au(111) electrode in contact 0.1 M H_2SO_4 + 0.1 mM Hg^{2+} (v = 1 mV s^{-1}). The inset shows the CV response after the potential is scanned to +0.48 V (v = 5 mV s^{-1})

duction peak appears around +0.55 V, as shown in the inset of Fig. 6. This peak corresponds to the reaction $2Hg^{2+} + 2e^- \leftrightarrow Hg_2^{2+}$ in bulk solution [30]. There is also a very sharp reduction spike at +0.48 V, which is superimposed on the broad reduction wave. A corresponding sharp oxidation peak is observed only if the scan direction is reversed right after it passes +0.48 V. Once the potential is scanned beyond the sharp spike at +0.48 V, the sharp anodic peak disappears and both the sharp peaks around +0.90 V and the single cathodic peak at +0.48 V are dramatically broadened and diminished in amplitude in successive scans [5]. This change is clearly evident when comparing the inset with the main panel of Fig. 6. The sharp spike at +0.48 V likely indicates the completion of the Hg monolayer and the onset of amalgam formation.

In order to obtain structural information of the adsorbed species, we carried out grazing incident X-ray diffraction (GIXD) measurements at a series of potentials from +1.05 to +0.50 V at 50 mV intervals. Three ordered structures were observed in the potential ranges labeled A, B, and C in Fig. 6, respectively. Consistent with cyclic voltammetric features, a highly ordered adlayer structure (found to be a coadsorbed layer of mercurous sulfate (Hg_2SO_4); *vide infra*) was found between +0.80 and +0.88 V. Figure 7 shows the reciprocal space map of the observed in-plane diffraction spots from one of the domains of the coadsorbed UPD layer (open squares in Fig. 7(a)). This structure layer has an oblique unit cell with vector **a** aligned in the next-nearest-neighbor (NNN) direction of the Au(111) surface and vector **b** rotated by −6.3° from the NNN direction. This structure is similar to that reported by Itaya *et al.* by STM [30], but it is at odds with those found by Gewirth *et al.* by AFM [31].

When the potential was changed to approximately +0.68 V (the onset of the broad diffusional reduction wave), an ordered hexagonal structure corresponding to a Hg UPD adlayer (referred to as UPD Phase I) was found. This structure was transformed to a second ordered hexagonal structure (referred to as UPD Phase II) when the potential was moved to values below +0.63 V but above that

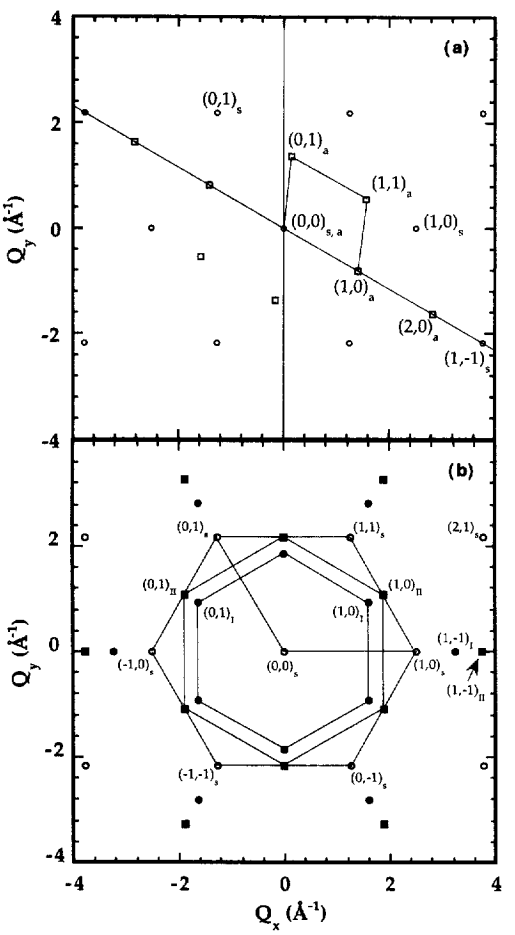

Fig. 7. (a) Reciprocal space map of the in-plane diffraction of the coadsorbed structure (open squares) relative to that of Au(111) surface (open circles). (b) Reciprocal space map of the in-plane diffraction from Hg UPD Phase I (solid circles) and Hg UPD Phase II (solid squares) relative to that of Au(111) surface (open circles). The reflections are indexed as $(h,k)_s$ for the Au(111) surface, $(h,k)_a$ for the coadsorbed structure, $(h,k)_I$ for Hg UPD Phase I, and $(h,k)_{II}$ for Hg UPD Phase II, respectively

of bulk deposition (around +0.45 V). The in-plane diffraction map for both phases is shown in Fig. 7(b). Both Hg UPD Phases I and II have hexagonal lattices rotated by 30° relative to the Au(111) substrate orientation. Whereas Phase II was found to be commensurate with the Au(111) substrate, Phase I was not. For both structures, higher order reflections at $(1,-1)_I$, $(2,1)_I$ and $(1,-1)_{II}$, $(2,1)_{II}$ were also observed, which unambiguously defined the hexagonal lattices of the Hg UPD adlayers. The diffraction peak positions of all these three phases were almost independent of the applied electrode potential.

The real space lattice can be directly calculated from the measured reciprocal lattice. From such analysis it was found that the coadsorbed overlayer has an oblique unit cell with $a = 4.197 \pm 0.0026$ Å, $b = 4.996 \pm 0.0036$, and $\alpha = 66.3°$ and that vector **b** is along the NNN direction of Au(111) surface atoms. In the coadsorbed Hg UPD layer, lattice b is exactly $\sqrt{3}\,a_s$ while lattice a is compressed by 16% and rotated by −6.3° from $\sqrt{3}\,a_s$. Hg UPD Phases I and II form hexagonal structures with $a = b = 3.86 \pm 0.03$ Å, $\alpha = 60°$, and $a = b = 3.34 \pm 0.01$ Å, $\alpha = 60°$.

In addition to these structures found by X-ray diffraction measurements, at potentials positive to the mercury UPD, a $(\sqrt{3}\times\sqrt{7})$ (bi)sulfate structure has been reported by STM measurements [30].

In order to investigate the nature of the adsorbed adlayers we carried out CTR measurements for an Au(111) electrode in 0.10 M H_2SO_4 containing 0.10 mM Hg^{2+} at potential values of +1.00, +0.80, +0.68 and +0.63 V (Fig. 8), the parameters obtained from data fitting at the different potentials are presented in Table 2 (a full description of the fitting procedure is given in Ref. [32]).

At E = + 1.00 V, the CTR data were virtually identical to those measured in pure 0.10 M H_2SO_4 solution at the same potential [11]. The data could be fitted with a monolayer of sulfate/bisulfate of a density $\rho_{ads} = 0.371 \pm 0.02$ which corresponds to either a 0.40 ML of bisulfate or a 0.20 ML of sulfate incorporating at least 0.40 ML of water or hydronium ions.

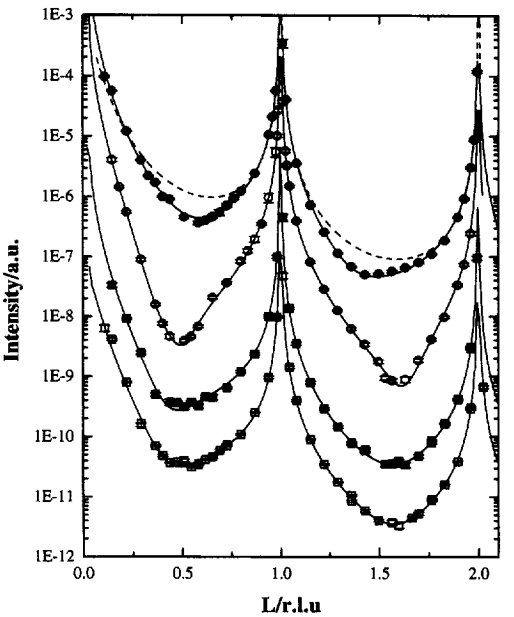

Fig. 8. CTR measurements of an Au(111) electrode in 0.10 M H_2SO_4 containing 0.10 mM Hg^{2+} measured at E = + 1.00 V (filled circles), +0.80 V (open circles), +0.68 V (filled squares) and +0.63 V (open squares) respectively. The dashed line is the calculated CTR curve from an ideally truncated Au(111) crystal. The continuous lines are the fits to the experimental data. Each profile is shifted by one order of magnitude relative to the previous one for a clearer view

The best fit to the data at +0.80 V required two adsorbate layers and the parameters obtained are presented in Table 2. Those values are consistent with a model in which the surface consists of

Table 2.
Specular CTR fitting parameters in 0.10 M sulfuric acid containing 0.10 mM Hg^{2+} ions at different potentials where ρ_n is defined as the atomic ratio of the species in the nth layer to that of Au atoms in a bulk Au(111) layer, σ_n the atomic root-mean-square displacement, and d the interlayer distance from the nth layer to the $(n-1)$th layer

E (V)	Topmost Au(111) layer	1st adsorbate layer	2nd adsorbate layer
+1.00	$\rho_0 = 1$, $\sigma_0 = 0.184 \pm 0.012$ Å, $d_0 = 2.406 \pm 0.004$ Å	$\rho^a_{ads} = 0.371 \pm 0.02$, $\sigma^a_{ads} = 0.2$ Å, $d^a_{ads} = 2.082 \pm 0.038$ Å	–
+0.80	$\rho_0 = 1$, $\sigma_0 = 0.2162 \pm 0.0046$ Å, $d_0 = 2.3125 \pm 0.0028$ Å	$\rho^b_{ads,1} = 0.616 \pm 0.012$, $\sigma^b_{ads,1} = 0.505 \pm 0.026$ Å, $d^b_{ads,1} = 2.457 \pm 0.018$ Å	$\rho^a_{ads,2} = 0.254 \pm 0.041$, $\sigma^a_{ads,2} = 0.66 \pm 0.17$ Å, $d^a_{ads,2} = 2.641 \pm 0.057$ Å
+0.68	$\rho_0 = 1$, $\sigma_0 = 0.165 \pm 0.007$ Å, $d_0 = 2.338 \pm 0.0066$ Å	$\rho^b_{ads} = 0.332 \pm 0.014$, $\sigma^b_{ads} = 0.44 \pm 0.06$ Å, $d^b_{ads} = 2.558 \pm 0.022$ Å	–
+0.63	$\rho_0 = 1$, $\sigma_0 = 0.178 \pm 0.0079$ Å, $d_0 = 2.349 \pm 0.0068$ Å	$\rho^b_{ads} = 0.38 \pm 0.11$, $\sigma^b_{ads} = 0.75 \pm 0.26$ Å, $d^b_{ads} = 2.46 \pm 0.14$ Å	–

[a]Fitted with a SO_4^{2-} or HSO_4^- layer.
[b]Fitted with a Hg layer.

ordered bilayer domains of Hg_2SO_4 and disordered monolayer domains. In this structure, the mercury species are adsorbed directly on the electrode surface and the (bi)sulfate layer is adsorbed on top of the mercury layer.

The CTR curves at +0.68 and +0.63 V, corresponding to UPD Phases I and II were about the same but quite different from both those at +1.00 and +0.80 V. In contrast to the two-layer structure at +0.80 V, the CTR data of these two phases can be fitted with a single Hg overlayer on the relaxed Au(111) surface. Values of the parameters from the best fit are presented in Table 2. The averaged densities of the Hg overlayers in both UPD phases are much lower than the values of 0.56 (Hg UPD Phase I) and 0.751 (Hg UPD Phase II) calculated from the in-plane structures. This suggests that both Hg UPD Phases I and II form two-dimensional islands on the Au(111) surface.

Figure 9(a) presents the real space structure of the co-adsorbed layer which is very similar to (but uniaxially compressed and rotated) the $(\sqrt{3}\times\sqrt{3})R30^\circ$ honeycomb structure of Cu UPD on Au(111) in sulfuric acid solutions [33]. The distortion is likely due to the formation of mercurous dimers (Hg_2^{2+}) which in Fig. 9(a) are arranged as pairs oriented along the same direction. The sulfate anions are adsorbed above the hollow sites of the Hg layer with two oxygen atoms pointing up and two down. As indicated in Fig. 9(a), the two oxygen atoms that are pointing down bond directly to the Hg atoms in two nearby Hg_2^{2+} dimers to form chemically linked zigzag rows along lattice vector **b**. We believe that this arrangement greatly stabilizes the overlayer structure.

Figure 9(b) and (c) are the schematic real space lattices of Hg UPD phases I and II, respectively. Both phases present hexagonal structures which are rotated by 30° relative to the substrate orientation. Hg UPD Phase I is incommensurate with the substrate whereas Hg UPD Phase II appears to form a $c(2\times 2)$ commensurate structure. The lattice of Hg UPD Phase I is expanded by 28.2% from the closest Hg–Hg distance which is likely due to the electrostatic repulsion between the partially charged Hg atoms. Hg UPD Phase II is more compact and stable with the mercury atoms being almost completely discharged. In addition, if the electrode potential is held at +0.63 V for more than 12 h, Hg UPD Phase II layer is further transformed into

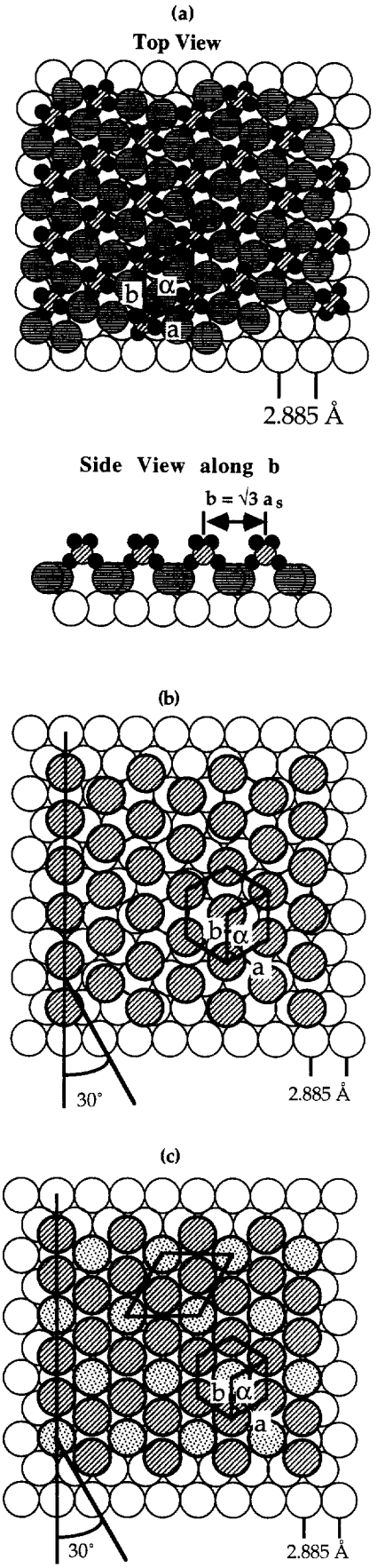

Fig. 9. (a) Schematic real space model of (a) the coadsorbed distorted honeycomb structure, (b) Hg UPD Phase I, and (c) Hg UPD Phase II, respectively. The large open circles represent the Au atoms on the substrate surface, the hatched and dot filled circles are the Hg overlayer atoms, and the small hatched circles attached by four solid circles represent sulfate anions

what appears to be either a 2D liquid Hg monolayer or a monolayer of an amorphous Hg–Au alloy [34].

Overall, our results in sulfuric acid indicate that the deposition process can be described by four steps:

$$2Hg^{2+}_{soln.} + (SO_4^{2-})_{ads} + 2e^- \leftrightarrow ((Hg_2)SO_4)_{ads} \quad (1)$$

$$((Hg_2)SO_4)_{ads} + 0.47e^- \leftrightarrow Hg/UPD - I \quad (2)$$

$$Hg/UPD - I + 0.53e^- \leftrightarrow Hg/UPD - II \quad (3)$$

$$Hg/UPD - II \leftrightarrow Hg^0/UPD \quad (4)$$

where $Hg^{2+}_{soln.}$, $((Hg_2)SO_4)_{ads}$, Hg/UPD-I, Hg/UPD-II and Hg^0/UPD represent, respectively, mercuric ions in solution, adsorbed mercurous sulfate, UPD Phases I and II, and the metallic mercury overlayer. This is in good agreement with the multistep mechanism proposed by potentiostatic measurements with a polycrystalline Au electrodes [35–38].

In the present system, a clear correlation between the partial charge retained by the deposited metal and the anion can be made. At the early stages of the electrodeposition, mercury has retained part of its charge, to give a Hg(I) species, which normally form Hg_2^{2+} dimers. A strong electrostatic interaction then appears between the charged metal and the sulfate anions present in solution that leads to the formation of an ordered layer of Hg_2SO_4 on the electrode surface, in a similar way to the CuCl layer formed on Pt(111) electrodes during Cu UPD in the presence of chloride anions as mentioned earlier. When the potential is made more negative, the partial charge on the metal diminishes, so that the interactions with the anions become weaker, leading to the disruption of the ordered bilayer formed. As metallic mercury has a low affinity for the (bi)sulfate anions [39], no anion layer is specifically adsorbed on the top of the deposited mercury when the mercury atoms are almost fully discharged (when Phase I and II are found on the electrode surface). These results are in contrast with those obtained for Cu UPD on Pt(111) in the presence of chloride. In this latter case, even at potentials close to bulk deposition and where Cu atoms are almost completely discharged, a chloride layer is always adsorbed on top of the deposited Cu. The difference in behavior arises from the fact that chloride anions adsorb strongly onto metallic copper.

CONCLUSIONS

We have presented three cases which illustrate the dramatic effects that anions and electrode surface structure can have in the structural and dynamical aspects of UPD processes. These effects include the adsorption of anions induced by a deposited (at step sites) metal layer, differences in the time scales of deposition vs long-range surface ordering and charge-state dependent structures. These studies demonstrate the delicate interplay that all of these effects have on UPD process.

ACKNOWLEDGEMENTS

This work was supported by the Office of Naval Research (U.S.A.), the National Science Foundation (U.S.A.), the Materials Science Center at Cornell University (U.S.A.) and the DGES (Spain). E. H. acknowledges support by a fellowship from the M.E.C. of Spain.

REFERENCES

1. D. M. Kolb, in *Advances in Electrochemistry and Electrochemical Engineering*, Vol. 11, ed. H. Gerischer and C. W. Tobias. Wiley, New York, 1978, p. 125.
2. R. Adzic, in *Advances in Electrochemistry and Electrochemical Engineering*, Vol. 13, ed. H. Gerischer and C. W. Tobias. Wiley, New York, 1978, p. 159.
3. N. Markovic and P. N. Ross, *Langmuir* **9,** 580 (1993).
4. Z. Shi, S. Wu and J. Lipkowski, *Electrochim. Acta* **40,** 9 (1995).
5. E. Herrero and H. D. Abruña, *Langmuir* **13,** 4446 (1997).
6. E. Herrero and H. D. Abruña, *J. Phys. Chem.*, accepted.
7. A. Tadjeddine, G. Tourillon and D. Guay, *Electrochim. Acta* **36,** 1859 (1991).
8. S. Wu, J. Lipkowski, T. Tyliszczak and A. P. Hitchcock, *Prog. Surf. Sci.* **50,** 227 (1995).
9. H. S. Yee and H. D. Abruña, *Langmuir* **9,** 2460 (1993).
10. H. S. Yee and H. D. Abruña, *J. Phys. Chem.* **97,** 6278 (1993).
11. J. Li and H. D. Abruña, *J. Phys. Chem. B* **101,** 244 (1997).
12. M. F. Toney, J. N. Howard, J. Richer, G. L. Borges, J. G. Gordon and O. R. Melroy, *Phys. Rev. Lett.* **75,** 4772 (1995).
13. I. M. Tidswell, C. A. Lucas, N. M. Markovic and P. N. Ross, *Phys. Rev. B* **51,** 10205 (1995).
14. R. Gómez, J. M. Feliu and H. D. Abruña, *J. Phys. Chem.* **98,** 5514 (1994).
15. R. Gómez, J. M. Feliu and H. D. Abruña, *Langmuir* **10,** 4315 (1994).
16. J. Clavilier, D. Armand, S. G. Sun and M. Petit, *J. Electroanal. Chem.* **205,** 267 (1986).
17. A. Rodes, K. El Achi, M. A. Zamakhchari and J. Clavilier, *J. Electroanal. Chem.* **295,** 333 (1990).
18. R. Gómez and J. Clavilier, *J. Electroanal. Chem.* **354,** 189 (1993).
19. M. G. Samant, M. F. Toney, G. L. Borges, L. Blum and O. R. Melroy, *Surf. Sci.* **193,** L29 (1988).
20. B. M. Ocko, J. Wang, A. Davenport and H. Isaacs, *Phys. Rev. Lett.* **65,** 1466 (1990).
21. J. Wang, B. M. Ocko, A. J. Davenport and H. S. Isaacs, *Phys. Rev. B* **46,** 10321 (1992).
22. R. R. Adzic, F. Feddrix, B. Z. Nikolic and E. Yeager, *J. Electroanal. Chem.* **341,** 287 (1992).
23. L. J. Buller, E. Herrero, R. Gómez, J. M. Feliu and H. D. Abruña, *J. Chem. Soc. Faraday Trans.* **92,** 3757 (1992).
24. J. Clavilier, K. El Achi and A. Rodes, *J. Electroanal. Chem.* **272,** 253 (1989).
25. R. Parsons and G. Ritzoulis, *J. Electroanal. Chem.* **318,** 1 (1991).

26. D. M. Kolb, A. Jaaf-Golze and M. S Zei, *Dechema Monographien (VCH, Germany)* **102,** 53–64 (1986).
27. H. Matsumoto, J. Inukai and M. Ito, *J. Electroanal. Chem.* **379,** 223 (1994).
28. R. Gómez, H. S. Yee, G. M. Bommarito, J. M. Feliu and H. D. Abruña, *Surf. Sci.* **335,** 101 (1995).
29. J. H. White and H. D. Abruña, *J. Phys. Chem.* **94,** 894 (1990).
30. J. Inukai, S. Sugita and K. Itaya, *J. Electroanal. Chem.* **403,** 159 (1996).
31. C.-H. Chen and A. A. Gewirth, *Phys. Rev. Lett.* **68,** 1571 (1992).
32. J. Li, E. Herrero and H. D. Abruña, *Coll. and Suf. A*, accepted.
33. M. F. Toney, J. N. Howard, J. Richer, G. L. Borges, J. G. Gordon, O. R. Melroy, D. Yee and L. B. Sorensen, *Phys. Rev. Lett.* **75,** 4472 (1995).
34. J. Li and H. D. Abruña, *J. Phys. Chem. B* **101,** 2907 (1997).
35. G. Salié and K. Bartels, *J. Electroanal. Chem.* **245,** 21 (1998).
36. K. Batels and G. Salié, *Z. Phys. Chem.* **271,** 739 (1990).
37. G. Salié, *J. Electroanal. Chem.* **259,** 315 (1989).
38. G. Salié, *J. Electroanal. Chem.* **259,** 315 (1989).
39. P. Delahay, *Double layer and electrode kinetics.* Interscience, New York, 1965, p. 61.